Journal of Power Sources 374 (2018) 113–120

Contents lists available at ScienceDirect

Journal of Power Sources

journal homepage: www.elsevier.com/locate/jpowsour

Introducing catalyst in alkaline membrane for improved performance direct borohydride fuel cells

Haiying Qin[a,*], Longxia Lin[a], Wen Chu[b], Wei Jiang[b], Yan He[c], Qiao Shi[e], Yonghong Deng[e], Zhenguo Ji[a], Jiabin Liu[b], Shanwen Tao[d,**]

[a] College of Materials and Environmental Engineering, Hangzhou Dianzi University, Hangzhou 310018, PR China
[b] School of Materials Science and Engineering, Zhejiang University, Hangzhou 310027, PR China
[c] Shanghai Synchrotron Radiation Facility, Shanghai Institute of Applied Physics, Chinese Academy of Sciences, Shanghai 201800, PR China
[d] School of Engineering, University of Warwick, Coventry, CV4 7AL, UK
[e] Shenzhen Capchem Technology Co., LTD, Shenzhen 518118, China

HIGHLIGHTS

- Catalyst was introduced in composite alkaline membrane uses as electrolyte for DBFC.
- Addition of catalyst increased ionic conductivity of membrane.
- Addition of catalyst reduced fuel cross-over and electrode polarization.
- DBFC using that membrane achieved OCV 1.11 V and P_{max} = 166 mW cm^{-2} at 30 °C.
- Idea of adding catalyst in membrane may apply in other electrochemical devices.

GRAPHICAL ABSTRACT

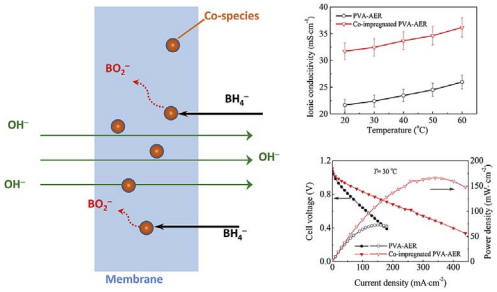

ARTICLE INFO

Keywords:
Alkaline polymer electrolyte membrane
Direct borohydride fuel cell
Ionic conductivity
Performance
Electrochemical impedance spectroscopy

ABSTRACT

A catalytic material is introduced into the polymer matrix to prepare a novel polymeric alkaline electrolyte membrane (AEM) which simultaneously increases ionic conductivity, reduces the fuel cross-over. In this work, the hydroxide anion exchange membrane is mainly composed of poly(vinylalcohol) and alkaline exchange resin. $CoCl_2$ is added into the poly(vinylalcohol) and alkaline exchange resin gel before casting the membrane to introduce catalytic materials. $CoCl_2$ is converted into CoOOH after the reaction with KOH solution. The crystallinity of the polymer matrix decreases and the ionic conductivity of the composite membrane is notably improved by the introduction of Co-species. A direct borohydride fuel cell using the composite membrane exhibits an open circuit voltage of 1.11 V at 30 °C, which is notably higher than that of cells using other AEMs. The cell using the composite membrane achieves a maximum power density of 283 mW cm^{-2} at 60 °C while the cell using the membrane without Co-species only reaches 117 mW cm^{-2} at the same conditions. The outstanding performance of the cell using the composite membrane benefits from impregnation of the catalytic Co-species in the membrane, which not only increases the ionic conductivity but also reduces electrode polarization thus improves the fuel cell performance. This work provides a new approach to develop high-performance fuel cells through adding catalysts in the electrolyte membrane.

* Corresponding author.
** Corresponding author.
E-mail addresses: hyqin@hdu.edu.cn (H. Qin), S.Tao.1@warwick.ac.uk (S. Tao).

https://doi.org/10.1016/j.jpowsour.2017.11.008
Received 30 July 2017; Received in revised form 19 October 2017; Accepted 2 November 2017
Available online 14 November 2017

1. Introduction

The ever-increasing demand on powering portable devices has generated a worldwide effort towards the development of high-energy-density power sources [1]. Polymer electrolyte membrane fuel cells (PEMFCs) have attracted increasing interest as promising power sources for portable and transportation applications because of their high energy densities, low operating temperatures and ease of transportation and storage [2–4]. As a key component, PEMFCs including direct borohydride fuel cells (DBFCs) use an electrolyte membrane (a proton or hydroxide conducting polymer membrane) to separate the anode from the cathode as well as to conduct reactants such as proton (H^+ cations) for acidic fuel cells or hydroxide ion (OH^- anions) for alkaline fuel cells. Currently used electrolyte membrane was mainly fluoropolymer based materials such as Nafion, developed by DuPont. Although the Teflon-like molecular backbones give those materials excellent long-term stability in both oxidative and reductive environments, the fuel cells using Nafion membrane suffered from using expensive precious cathode catalyst and some technological problems [1,3,5].

On the other hand, alkaline polymer electrolyte membranes (AEMs), in which the charge carriers are OH^- ions rather than protons, have been considered as an attractive electrolyte membrane regarding the fast fuel cell reaction kinetics and application of non-precious metal catalysts [3,6–8]. However, there are still some challenges with AEMs. The ionic conductivity of AEMs is lower than that of Nafion membrane. The cells using AEMs suffer from fuel cross-over from anode to cathode and insufficient stability as well as carbonation [3]. To overcome these challenges, tremendous effort should be put into improving the ionic conductivity and stability and reducing the fuel cross-over.

It is well known that mixing some inorganic materials into a polymer matrix will change the mechanical, thermal and chemical properties [9]. Using a solution casting method, Li et al. prepared quaternized poly(arylene ether sulfone)/nano ZrO_2 composites with high hydroxide ion conductivities over 41.4 $mS{\cdot}cm^{-1}$ at 80 °C [10]. Recently, Liu et al. grafted Fe_3O_4 nanoparticles on carbon nanotubes (CNTs) and then added them into Nafion or poly(vinyl alcohol) (PVA) matrix to prepare hybrid membrane. The direct methanol fuel cell using the hybrid membrane exhibited higher proton conductivity, lower methanol permeability, and higher peak power density than the pristine Nafion or PVA membranes [10,11]. Further studies indicate that the addition of inorganic fillers into a polymer matrix facilitates a reduction in the glass transition temperature and the crystallinity of the polymer. Therefore, the amorphous phases of the polymer matrix as well as the ionic conductivity, are increased.

High ionic conductivity is the most important property of an electrolyte. However, simple improvement of ionic conductivity of the AEMs is hard to solve the cross-over problem. It may be interesting to see what will happen if catalytic inorganic materials were added into the polymer matrix.

It has been reported that anion exchange resin (AER) and PVA composite membrane can be used as an electrolyte for alkaline fuel cells [12,13]. However, the conductivity of PVA-AER composite membrane was not reported. In this work, $CoCl_2$ was introduced into the PVA-based membrane, and the membrane was used as an electrolyte in the DBFC. $CoCl_2$ was further converted into CoOOH after the reaction with KOH solution. It is interesting to find that the DBFC using that membrane exhibits much better performance than the DBFC using Nafion N117 membrane. The key reason is attributed to the combination of improved ionic conductivity and reduced cross-over of the electrolyte membrane. A new strategy for the design of high-performance membrane for fuel cell applications is proposed.

2. Experimental

2.1. Preparation of alkaline membrane

The composite alkaline membrane was prepared from a commercial strong AER (Amberlite IRA-402(OH), hydroxide form, Alfa Aesar) and PVA (MW 57000–66000, Alfa Aesar) at a weight ratio of 1:2. PVA was dissolved in de-ionized water and stirred at 95 °C for 2 h to form a gel. After the gel was cooled down to room temperature, the commercial AER powder was mixed with PVA gel to form the wet composite polymer gel. The wet composite polymer gel was cast on a glass plate, and the thickness of the wet gel on the plate was controlled at about 1 mm. The wet gel dried naturally at room temperature to form a PVA-AER blend membrane.

The $CoCl_2$-added composite alkaline membrane (Co-impregnated PVA-AER) was made by adding $CoCl_2{\cdot}6H_2O$ into the PVA gel at a weight ratio of 2:125 before mixing with AER. The nominal percent of the $CoCl_2$ impregnated into the membrane was 0.4 wt% and 1.0 wt%. The following processes were similar to those of PVA-AER membrane. The thickness of the dried PVA-AER and Co-impregnated PVA-AER membrane was about 200 μm. The schematic diagram for the preparation of the membranes was shown in Fig. S1. All the dried membranes were immersed in 1 M KOH solution up 24 h. Then the membranes were washed several times with de-ionized water and stored in the de-ionized water before use.

2.2. Microstructure characterization

The crystal structure of the synthesized membranes was identified by X-ray diffractometer (XRD, Philips X'PERT-PRO) with Cu *K*α radiation. The microstructure of the membranes was investigated by scanning electron microscopy (SEM, Hitachi SU70). The composition was tested by an energy dispersive spectrometer (EDS) equipped in a SEM (Hitachi S3400) operated at 15 kV. The X-ray absorption near edge structure (XANES) measurements were performed on BL14W in Shanghai Synchrotron Radiation Facility (SSRF). The electron beam energy of the storage ring at SSRF was 3.5 GeV, and the maximum stored current was about 210 mA. All measurements for XANES were performed in fluorescent mode, and a dwell time of 2 s was used to collect the fluorescent signals for each energy point. The fluorescent signals induced by the injected X-ray were recorded by the fluorescent detector. X-ray photoelectron spectroscopy (XPS) was carried out on a Thermo Fisher Scientific, Escalab 250Xi. The thermal stability of the prepared membrane was analyzed using a different scanning calorimetry and thermogravimetric analyzer (DSC-TGA, SDT Q600, TA Instrument, USA). Measurements were carried out by heating from room temperature to 700 °C at a heating rate of 5 $°C{\cdot}min^{-1}$ with about 10 mg sample under N_2 atmosphere with a N_2 flow rate of 20 $mL{\cdot}min^{-1}$. The water uptake of the dried membrane was ~15% based on the TGA results.

2.3. Physicochemical characteristics

To get the alkaline uptake (*AU*) and swelling degree (*SD*), both the weight and the dimension of dry membranes (denoted as m_{dry} and L_{dry}) were measured before immersed in 1 M KOH solution at 30 °C for 48 h. Then the membrane was washed with deionized water several times to remove residual KOH and wiped dry with lens paper. The wet mass m_{wet} and the dimension L_{wet} of the membranes were measured. The *AU* and the *SD* were calculated by:

$$AU(\%) = \frac{m_{wet} - m_{dry}}{m_{dry}} \times 100 \quad (1)$$

$$SD(\%) = \frac{L_{wet} - L_{dry}}{L_{dry}} \times 100 \quad (2)$$

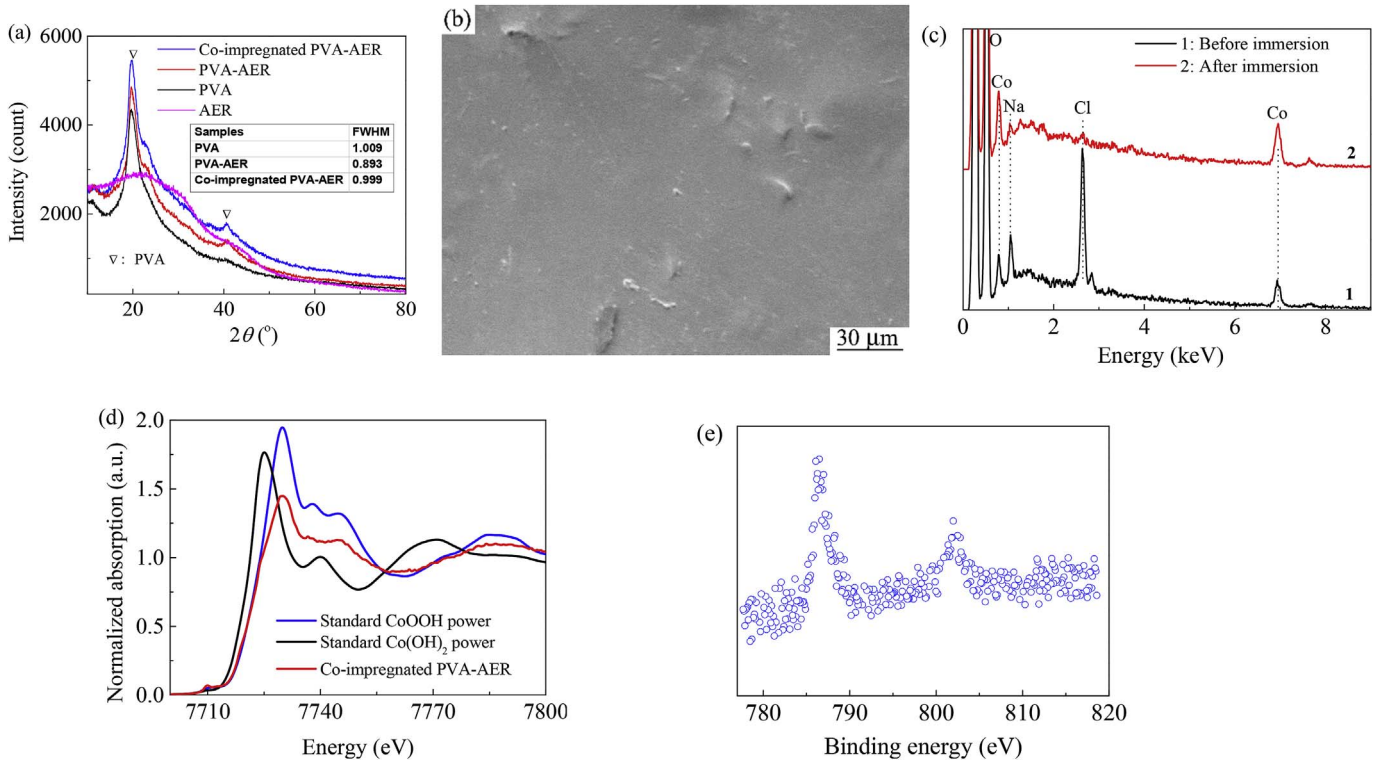

Fig. 1. (a) XRD spectra of the AER, PVA, PVA-AER membrane and Co-impregnated PVA-AER membrane, the FWHM of the peak at about 20° is given as inserted table, (b) SEM image of the Co-impregnated PVA-AER membrane, (c) EDS spectra of the Co-impregnated PVA-AER membrane before and after immersion in KOH, (d) XANES spectra of Co element in the Co-impregnated PVA-AER membrane and standard CoOOH and $Co(OH)_2$ samples, (e) XPS Co 2p spectra for the Co-impregnated PVA-AER membrane.

The measure method of the ionic conductivity and the testing device could be found elsewhere [5]. A piece of membrane (6 cm^2 in area) was assembled in the testing device, which connected to the working and reference electrodes of a potentiostat (Gamry interface 1000, USA). The measurements were conducted at the temperature ranging from 20 to 60 °C using a two-probe AC-impedance method under fully humidified atmosphere. The membrane resistance was measured over a frequency range of 0.01 Hz–1 MHz with an oscillating voltage amplitude of 5 mV. The ionic conductivity (σ) was calculated by:

$$\sigma = \frac{t}{R_{mem} \times A} \quad (3)$$

where t was the membrane thickness, R_{mem} was the membrane resistance, and A was the electrode area.

The borohydride ion permeability was tested by a side-by-side diffusion cell at 20 °C. Both sides were first filled with a solution of 50 mL 0.1 M NaOH; then extra 0.1 M $NaBH_4$ was only added to one side. The borohydride ion concentration in the receiving compartment was measured by using the spectrophotometric method proposed by Werner et al. [14]. In a typical assay procedure, 0.3 mL solution in the receiving compartment was taken and mixed with 2.7 mL nicotinamide adenine dinucleotide (NAD^+) reagent which was prepared by 0.05 M NAD+ and 0.05 M tris(hydroxymethyl)amino methane buffer solution (pH of 8.5) at a volume ratio of 1:17. The mixture solution was reacted for 15 min at 20 °C and then tested by a spectrophotometry (Shimadzu UV3600) operated at a wavelength range between 400 and 300 nm. The valence of the Co element was clarified by XPS. The borohydride ion concentration was calculated with the help of the calibration curves whose R^2 value was 0.9995 (Fig. S2). The permeability (P) was calculated by Ref. [15].

$$P = (\text{slope})\frac{LV}{CA} \quad (4)$$

where the slope is the permeated borohydride ion concentration against elapsed time, L the thickness of the tested membrane, V the volume of the receiving compartment, C the concentration of the initial borohydride and A the effective area of the tested membrane [15].

2.4. Fuel cell performance

The anode was prepared by coating a catalyst paste onto a piece of Ni foam with a catalyst loading of 5 mg cm^{-2}. The anode catalyst paste was prepared by mixing polypyrrole modified carbon supported cobalt hydroxide ($Co(OH)_2$-PPy-BP) and Nafion suspension (5 wt%) at a mass ratio of 1:7. Cathodes were prepared by coating a catalyst slurry onto a piece of hydrophobic carbon cloth with a catalyst loading of 3 mg cm^{-2}. The cathode catalyst slurry was prepared by mixing Co $(OH)_2$-PPy-BP and polytrafluroethylene suspension at a mass ratio of 1:7. And then the cathode was sintered at 350 °C for 5 min.

A single cell with an effective area of 6 cm^2 was assembled to evaluate electrochemical performance of the membranes. The cell configuration and cell test system were described in a previous study [16]. The electrochemical properties of the PVA-AER and Co-impregnated PVA-AER membranes were compared at the same conditions. An alkaline $NaBH_4$ solution containing $NaBH_4$ (5 wt%) and NaOH (10 wt%) was used as fuel. Cell performance and polarization behaviour were evaluated using a PFX-2011 battery tester (Kikusui Electronics Corp.) at a fuel flow rate of 10 mL·min^{-1} and humidified O_2 flow rate of 100 mL·min^{-1} under 0.2 MPa. A calomel electrode was used as the reference electrode and connected with fuel tank by a salt bridge.

To obtain the membrane resistance, anode reaction and cathode reaction resistance of the fuel cell, AC impedance measurements were carried out by an Interface 1000 potentiostat (Gamry, USA). A perturbing amplitude of 5 mV in the whole frequency range of 0.01 Hz–10 kHz was employed. The testing currents were 0.3, 0.6 and 0.9 A at ambient condition. Software Z-View was used for the electrochemical AC impedance data analysis.

3. Results

3.1. Membrane characterization

The XRD results of the PVA, AER, PVA-AER and Co-impregnated PVA-AER membranes are given in Fig. 1(a). A strong peak at about 20° plus a weak at about 40° are observed for the PVA, and no obvious peak is detected for the AER. However, the peak at about 40° becomes stronger after adding AER into the PVA indicating there is some interaction between AER and PVA. The emergence of the peak at about 40° in the PVA-AER indicates that the crystallinity of the PVA matrix should be improved due to the interaction with AER. This deduction is also supported by the full width at half maximum (FWHM), which strongly reflects the crystallinity of the sample. The FWHM of the peak at about 20° is 1.009° for PVA and is 0.893° for PVA-AER. The addition of $CoCl_2$ does not introduce new peak in the XRD spectrum of the Co-impregnated PVA-AER. This phenomenon indicates that the Co-compound is not enough to be picked up by XRD or it is in the amorphous state. However, the FWHM of the peak at about 20° is notably increased to 0.999° in the Co-impregnated PVA-AER compared to that in the PVA-AER (0.893°). The increase in the FWHM strongly indicates that the crystallinity of the PVA matrix is reduced by the addition of $CoCl_2$. The morphology of the membranes was observed by SEM and is shown in Fig. 1(b) and Fig. S3. There is little difference between the PVA-AER and Co-impregnated PVA-AER membranes. Both membranes are relatively smooth, and few pores were observed. The composition of the Co-impregnated PVA-AER membrane before immersion in KOH mainly consists of C, O, Na, Cl and Co elements (Fig. 1(c)). The Na element comes from the AER. The existence of Cl and Co elements confirm the success of $CoCl_2$ addition into the polymer matrix. However, the Cl element disappears while the Co element remains in the membrane after immersion in KOH for 24 h then washed with water, as shown in Fig. 1(c). The K element was not detected even for the membrane after immersion because the membrane was washed by de-ionized water for several times after immersed in KOH for 24 h then the residual was removed. The EDS result indicates that the $CoCl_2$ should change into Co hydroxide or Co oxyhydroxide due to the strong alkaline environment. The XANES spectrum of the Co-impregnated PVA-AER membrane, together with the spectra of standard CoOOH and $Co(OH)_2$ samples, are shown in Fig. 1(d). The absorption energy and the position of the white line of the Co-impregnated PVA-AER membrane are similar to those of standard CoOOH sample, which indicates that the valence of Co atoms in the Co-impregnated PVA-AER membrane is +3. It should be pointed out that the initial valence of Co is +2 in $CoCl_2$. The change of the Co valence indicates that the $CoCl_2$ should evolve into CoOOH after immersed into 1 M KOH solution for 24 h. The XPS test was carried out to clarify the valence of the Co element in the membrane, and the result is shown in Fig. 1(e). Two peaks at about 786 eV and 802 eV are observed in the spectra. The binding energies of the Co 2p3/2 and the Co 2p 1/2 in CoOOH nanobelts were reported as 785.7 eV and 801.9 eV [17]. The binding energies of the Co 2p3/2 and the Co 2p 1/2 in CoOOH hollow spheres were reported as 786.5 eV and 802.4 eV [17]. The binding energies in this work are close to the results of the CoOOH nanobelts and the CoOOH hollow spheres, which supports the identification of CoOOH by XANES.

Fig. 2(a) and (b) show TGA and DSC analysis thermographs of the PVA-AER and Co-impregnated PVA-AER membranes, respectively. The TGA curves of both membranes can be divided into three weight loss stages. The first stage is from room temperature to 260 °C, which corresponds to the removal of residual water. The weight loss of the Co-impregnated PVA-AER membranes is almost the same as that of the PVA-AER membrane in the stage I. The second weight loss stage commencing around 260 °C is assigned to the degradation of quaternary ammonium groups and PVA membrane [18]. The weight loss of the Co-impregnated PVA-AER membrane (53.20 wt%) is less than that of the PVA-AER membrane (56.32 wt%) in stage II. The third weight loss stage at the temperature higher than 300 °C is assigned to the polymer backbone decomposition [10]. The weight loss of the Co-impregnated PVA-AER membranes is slightly less than that of the PVA-AER membrane in stage III. It is reasonable to conclude that the Co-impregnated PVA-AER membrane can retain more water at evaluated temperatures which should be attributed to the addition of the inorganic salt of $CoCl_2$ into the polymer matrix and the formation of CoOOH after the reaction with KOH solution. It is well documented that the inorganic filler phase is effective in improving the thermal stability of polymer composite [10,18]. The polymer crystallinity could be reflected by the enthalpy change in the DSC curves. The enthalpy change of the Co-impregnated PVA-AER membrane (18.56 J g^{-1}) is obviously less than that of the PVA-AER membrane (21.83 J g^{-1}) at about 260 °C, indicating lower crystallinity of the former. The DSC results are consistent with the former XRD results. It was reported that the introducing of hydrophilic hydroxyapatite ceramic filler would decrease the crystallinity and increase the amorphous phases of the polymer matrix [19]. Therefore, the decreased crystallinity of the Co-impregnated PVA-AER membrane should result from the incorporating of $CoCl_2$ in the PVA-AER matrix. It is expected that the ionic conductivity of the composite membrane will also change as it is related to the crystallinity of the membrane as well.

The temperature-dependent ionic conductivities of PVA-AER and Co-impregnated PVA-AER membranes are shown in Fig. 2(c). The ionic conductivity of Co-impregnated PVA-AER membrane is roughly 1.4 time of that of PVA-AER membrane in the measured temperature range. The ionic conductance is thought to be realized through several mechanisms: Grotthus (hopping), vehicular (bulk) diffusion, and surface diffusion [20]. The higher alkali uptake of the Co-impregnated PVA-AER membrane than the PVA-AER membrane (Table S2) should be beneficial to ion transport through the hopping mechanism. On the other hand, the $CoCl_2$ salt filler reduces the crystallinity of the polymer matrix (Fig. 2(b)) and creates free volume, which is also an advantage for improving ionic conductivity. Therefore, the ionic conductivity is notably enhanced by introducing a small amount of $CoCl_2$.

The absorption curves of the solution in the receiving compartment separated by the Co-impregnated PVA-AER membrane at time interval are shown in Fig. 3(a). There are typical peaks at about 350 nm of the curves, and the maximum absorbance is used to calculate the borohydride ion concentration with the help of calibration curves. The borohydride ion concentration dependent on the elapsed time is shown in Fig. 3(b). The slopes of the permeated borohydride ion concentration against elapsed time are 1.30 and 1.39 μM s^{-1} for the Co-impregnated PVA-AER membrane and the PVA-AER membrane, respectively. The thicknesses of the Co-impregnated PVA-AER membrane and the PVA-AER membrane are measured to be 233 ± 5 and 250 ± 5 μm. Therefore the permeabilities of both membranes are calculated to be 2.53 ± 0.09 × 10^{-6} and 2.90 ± 0.11 × 10^{-6} cm^2 s^{-1}, respectively. This indicates that addition of CoOOH catalyst can reduce the cross-over of borohydride fuel which is very beneficial for low-temperature fuel cells with liquid fuels. The decreased fuel cross-over may be related to the hydrolysis of borohydride by the addition of CoOOH.

The cell performances of the DBFCs using various membranes were measured at 30 and 60 °C and shown in Fig. 4, respectively. At 30 °C, the maximum power densities (P_{max}) obtained in the DFBCs using the Co-impregnated PVA-AER and the PVA-AER membranes are 166 and 72 mW cm^{-2}, respectively. The advantage of the Co-impregnated PVA-AER membrane is more obvious when the DBFC is working at higher temperatures. The DBFC using the Co-impregnated PVA-AER membrane achieves a P_{max} of 283 mW cm^{-2}, while the DBFCs using the PVA-AER only achieve a P_{max} of 117 mW cm^{-2}, respectively. Polarization measurements indicate that the DBFC using the Co-impregnated PVA-AER membrane has the smallest polarization among all test cells (Fig. S4) which may be beneficial from the improved catalytic activity at the triple phase boundary of both electrodes due to the addition of the Co-based catalyst in the electrolyte membrane. The durability test indicates that, for a fuel cell based on Co-impregnated PVA-AER

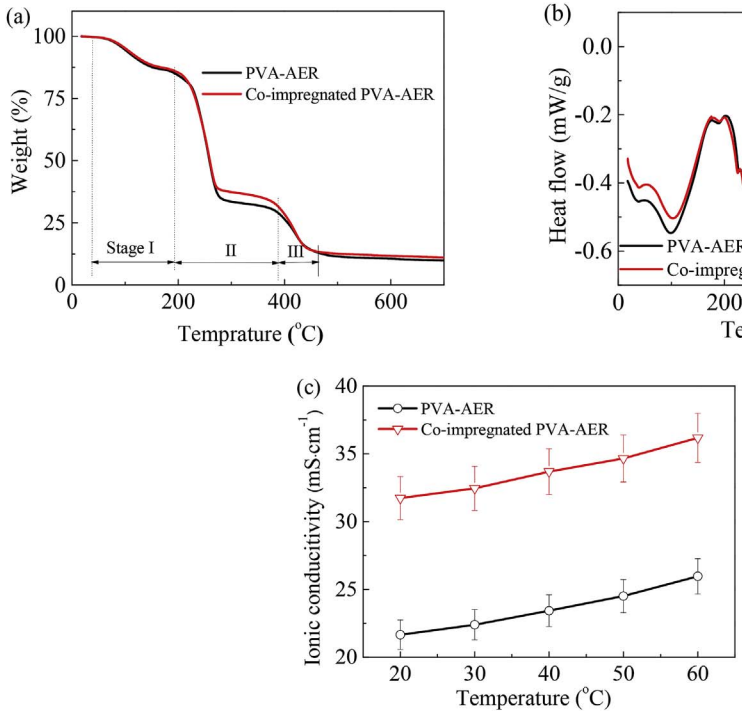

Fig. 2. (a) TGA and (b) DSC curves for the PVA-AER membrane and Co-impregnated PVA-AER membrane, (c) the temperature-dependent ionic conductivity of PVA-AER and Co-impregnated PVA-AER membrane.

membrane electrolyte, the cell voltage only decreases 7% when discharging at 50 mA cm^{-2} for 35 h (Fig. S5). Two review papers have given a completely summary of the performances of DBFC using AEM, Nafion membranes or other membranes [21,22]. Table 1 only shows the open circuit voltage (OCV) and P_{max} results of DBFCs suing AEM reported by different researchers. Many good results were obtained using precious catalysts such as Pt and Pt-Ru. In this work, the non-precious catalyst was used as both cathodes and anodes for DBFCs. It is interesting to find that our DBFCs based on the Co-impregnated PVA-AER membrane and non-noble catalysts outperform the performance of DBFC using precious catalysts and other AEMs under similar conditions. The OCVs of the DBFC using Co-impregnated PVA-AER membrane are 1.11 and 1.06 V at 30 and 60 °C, respectively. These values are higher than the reported results for AEM-DBFC in Table 1. This also demonstrates that electronic conduction in the Co-impregnated PVA-AER membrane is negligible.

Electrochemical impedance spectroscopy (EIS) measurement was carried out and shown in Fig. 5. Table 2 shows the quantitative EIS results of the DBFCs corresponding to Fig. 5(b) ~ (d). There are two arcs in the Nyquist plots of the DBFCs as shown in Fig. 5(a). The *X*-intercept represents the ohmic resistance of the electrolyte membrane together with all the external resistances (R_{ohm}), the diameter of the semi-circle at high frequencies is related to the electrochemical reaction on the anodes, the diameter of the semi-circle at low frequencies is related to the electrochemical reaction on the cathodes [23,24]. Since the electrodes used in the tested DBFCs are the same, the different EIS results mainly reflect the properties of the electrolyte materials. The DBFC based on the Co-impregnated PVA-AER membrane exhibits smaller ohmic resistance and the smaller activation resistance for both cathode and anode. The reduction of ohmic resistance and activation resistance for the DBFC using the Co-impregnated PVA-AER membrane should benefit from the addition of $CoCl_2$ and corresponding product of CoOOH.

The EIS results change significantly once the DBFCs are under galvanostatic mode. An equivalent circuit depicted and inserted in Fig. 5(b) was used to simulate the Nyquist plot using software Z-View. The R_{ohm}, $R_{f,a}$, $R_{f,c}$ and constant phase element (CPE) represent the ohmic resistance, the electrochemical reaction resistance of the anode, the electrochemical reaction resistance of the cathode and the R_f-associated catalyst layer capacitance properties, respectively [24]. The R_{ohm}, $R_{f,a}$ and $R_{f,c}$ of DBFCs using different membranes at different discharge current are listed in Table 2. The DBFC using the Co-impregnated PVA-AER membrane shows smaller R_{ohm} at every discharge current. Since the R_{ohm} represents the ohmic resistance of the electrolyte membrane mainly together with all the external resistances, it is obvious that the ohmic resistance of Co-impregnated PVA-AER is smaller than that of PVA-AER (Table 2). As the discharge current increases from 0.3 A to 0.9 A, the R_{ohm} of all the tested cells decreases. A

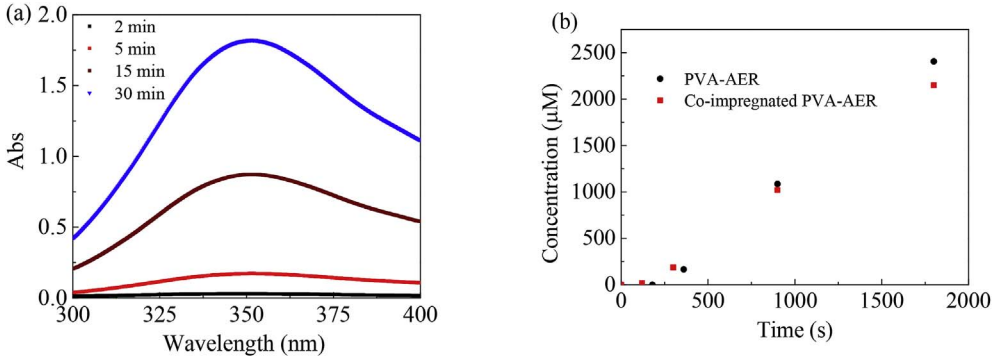

Fig. 3. (a) The absorption curves of the solution in the receiving compartment separated by the Co-impregnated PVA-AER membrane and (b) the borohydride ion concentration dependent on the elapsed time in the receiving compartment separated by the Co-impregnated PVA-AER membrane and the PVA-AER membrane.

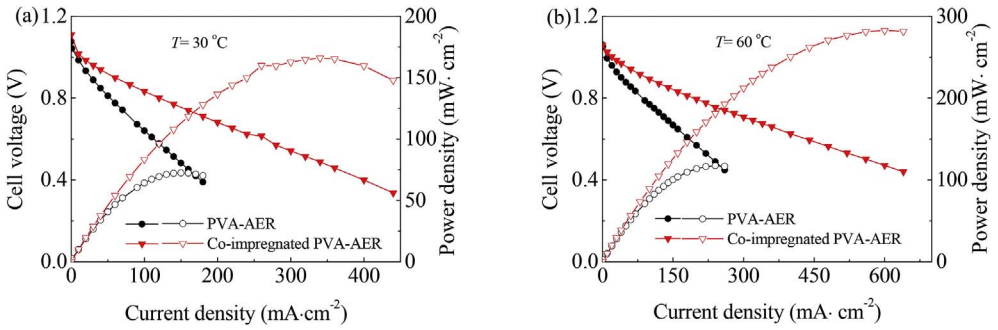

Fig. 4. Comparison of cell performances for the DBFCs operated with PVA-AER and Co-impregnated PVA-AER membranes operated at (a) 30 °C and (b) 60 °C.

Table 1
Comparison of P_{max} and OCV of DBFCs presented in the literature and this work.

Electrolyte	Anode catalyst	Cathode catalyst	T (°C)	Fuel	Oxidant	OCV (V)	P_{max} mW·cm^{-2}	References
PVA/hydroxyapatite	Pt-Ru/C	MnO_2/C	25	1 M KBH_4 + 4 M KOH	Air	About 1.15	45	Yang et al. [19]
NaOH-doped PVA	Pt-Ru/C	Pt	30	1 M $NaBH_4$ + 4 M NaOH	O_2	About 0.98	96	Huang et al. [15]
NaOH-doped PVA/CNT	Pt-Ru/C	Pt	30	1 M $NaBH_4$ + 4 M NaOH	O_2	About 0.98	91	Huang et al. [15]
Morgan ADP (solvay) AEM	Pt/C + Pt black	Non Pt-based	25	2 M $NaBH_4$ + 1 M NaOH	Air	0.89	200, 194	Jamard et al. [28,29]
Co-impregnated PVA-AER	Co(OH)$_2$-PPy-C	Co(OH)$_2$-PPy-C	30	5 wt% $NaBH_4$ + 10 wt% NaOH	O_2	1.11	166	This work
BG-BPS/PTFE	Pt/C	Pt/C	40	1 M $NaBH_4$ + 3 M NaOH	O_2	0.91	321	Qu et al. [30]
Alkali-doped poly (4, 4′-diphenylether-1, 3, 4-oxadiazole)	Pt/C	Pt/C	40	1 M $NaBH_4$ + 3 M NaOH	O_2	About 0.98	146	Mai et al. [31]
Polybenzimidazole-60	Pt/C	Pt/C	40	1 M $NaBH_4$ + 3 M NaOH	O_2	About 1.0	262	Chen et al. [32]
PVA hydrogel	Ni-Pd/C	Pt/C	60	5 wt% $NaBH_4$ + 10 wt% NaOH	O_2	About 1.05	242	Ma et al. [33]
Co-impregnated PVA-AER	Co(OH)$_2$-PPy-C	Co(OH)$_2$-PPy-C	60	5 wt% $NaBH_4$ + 10 wt% NaOH	O_2	1.06	283	This work

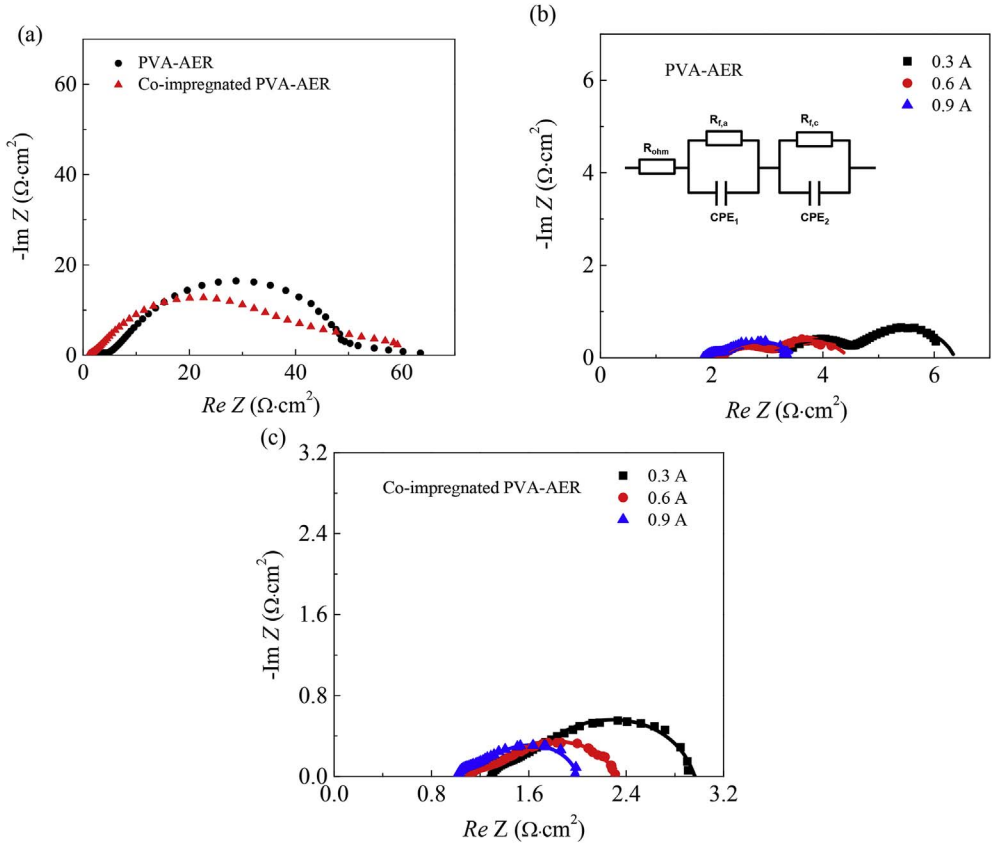

Fig. 5. (a) Nyquist plots of the DBFCs using the PVA-AER and Co-impregnated PVA-AER membranes before discharging, Nyquist plots of the DBFCs charged at a current of 0.3, 0.6 and 0.9 A (b) using the PVA-AER membrane and (c) using the Co-impregnated PVA-AER membrane. All the DBFCs use the same cathodes and anodes and are tested at 30 °C.

Table 2
The R_{ohm}, $R_{f,a}$ and $R_{f,c}$ of the DBFCs using different membranes at discharge current of 0.3, 0.6 and 0.9 A. Data were obtained from simulate the Nyquist plots of the DBFCs as shown in Fig. 5.

Membrane used	Discharge current (A)	Rohm ($\Omega \cdot cm^2$)	$R_{f,a}$ ($\Omega \cdot cm^2$)	$R_{f,c}$ ($\Omega \cdot cm^2$)
PVA-AER	0.3	3.432	1.382	1.741
	0.6	2.202	0.832	1.434
	0.9	1.878	0.296	1.371
Co-impregnated PVA-AER	0.3	1.182	0.670	1.115
	0.6	1.038	0.440	0.858
	0.9	0.984	0.396	0.624

similar trend was observed in proton exchange membrane fuel cells [25]. The $R_{f,a}$ and $R_{f,c}$ of the DBFCs using the Co-impregnated PVA-AER and PVA-AER membranes also decrease with increasing current. The decrease of the $R_{f,a}$ and $R_{f,c}$ of the DBFCs using the Co-impregnated PVA-AER and PVA-AER membranes indicates that increasing discharge current is favourable to speed up the reaction kinetics of the DBFCs. The $R_{f,a}$ and $R_{f,c}$ of the cell using the Co-impregnated PVA-AER membrane are much lower than those of the cell using the PVA-AER membrane. The reduction of reaction resistance for the DBFC using the Co-impregnated PVA-AER may benefit from the introduction of $CoCl_2$ since the cobalt compound is an effective catalyst towards borohydride [26,27]. This may be related to the improved catalytic activity on the electrolyte surface in contact with the triple phase boundary, which will be discussed later.

4. Discussions

The addition of $CoCl_2$ during the preparation of membranes would introduce Co compound in the polymer matrix. The possible composition of the Co compound is CoOOH since the alkaline solution is used in the following procedures. Due to the strong alkaline characteristics of AER and KOH, firstly $CoCl_2$ reacts with the OH^- to produce the $Co(OH)_2$. Then the formed $Co(OH)_2$ is further oxidized into CoOOH with the help of O_2 in the air and the alkaline environment [34,35]. The $Co(OH)_2 \rightarrow CoOOH$ oxidation reaction in KOH was reported to occur through a two-step mechanism process [35]. Therefore, Co species are present as Co oxyhydroxide in the Co-impregnated PVA-AER membrane. The presence of the CoOOH is confirmed by the XANES results that the spectrum of the Co-impregnated PVA-AER membrane is close to that of the standard CoOOH sample (Fig. 1(d)). The characteristics of no crystalline peak in XRD pattern indicates that CoOOH may be amorphous, which is reasonable since no reaction was carried out at high temperature. The presence of Co compound in the membrane may decrease the crystallinity and increase the free volume of the polymer matrix, leading to increased ionic conductivity. Therefore, the ionic conductivity of the Co-impregnated PVA-AER membrane is notably enhanced in comparison with the PVA-AER membrane. Similar successes in the increase of ionic conductivity of AEMs were obtained in several previous studies. For example, oxides (e.g. Al_2O_3, TiO_2, and ZrO_2), carbon nanotubes and CdSe quantum dot were added into a polymer matrix to change the mechanical, thermal and chemical properties of the membranes [9,10,15,18,36]. The key difference between the previous studies and this work is the function of the inorganic material. In most case, the introduction of inorganic materials into the polymer matrix is effective in improving the thermal stability and ionic conductivity while in this study the indirectly added CoOOH also improved the catalytic activity of the composite membrane, resulting in reduced electrode polarization resistances, decreased fuel cross diffusion and improved fuel cell performance.

Since the ionic conductivity of the membrane plays an important role in the cell performance, it is meaningful to enhance the ionic conductivity to improve the cell performance. The results shown in Figs. 4 and 5 verify that the outstanding performance of the DBFC using the Co-impregnated PVA-AER membrane profits from the small reaction resistance of the membrane.

Another unique benefit of the addition of $CoCl_2$ in comparison of others' work is the functionalization of the membrane by Co-species. An important purpose of the introduction of Co-species is to produce some catalytic activity in the membrane. It is well accepted that Co-species are effective catalysts towards oxidation and hydrolysis of borohydride [26,27]. The introduction of Co-species into the polymer matrix not only improves the ionic conductivity but also produces certain catalytic activity towards borohydride. Although both the OH^- and BH_4^- anions are transported through the PVA-AER membrane, the BH_4^- anions would be hydrolysed with the help of the Co-species in the membrane according to the flowing reaction:

$$BH_4^- + 2H_2O \xrightarrow{CoOOH} BO_2^- + 4H_2 \quad (5)$$

Therefore, the cross-over of the borohydride in the AEM-DBFCs will be reduced which is verified by the permeability results (Fig. 3(b)). The realization of lower permeability but higher ionic conductivity of the AEM highly benefits from the addition of CoOOH in the membrane. The Co-impregnated PVA-AER membrane with decreased fuel cross-over also contributes to the outstanding performance of the DBFC. Moreover, the introduction of catalyst in the membrane electrolyte may extend the electrochemical reactions at triple phase boundary at both cathode and anode, leading to reduced polarization resistance on both electrodes which are evidenced by the data in Fig. 5 and Table 2. This also leads to the increased OCV and improved fuel cell performance.

In fact, the cross-over is the principal limitation to the development of the AEM-DBFCs. The popular method to solve this problem is to suppress the conductivity of the BH_4^- anions. However, the suppression of the conductivity of the BH_4^- anions is always companied with the suppression of the conductivity of the OH^- anions. In this work, a novel method is provided that the BH_4^- anions are catalytically hydrolysed by the functionalized membrane. By this method, the number of the BH_4^- anions arrived at the cathode would be reduced while high anionic conductivity remains or even increases. It should be pointed out that this method could not improve the fuel utilization and faradic efficiency. However, this method reduces the effective cross-over and improves the cell performance. The OCV presented in Table 1 confirms the validity of this method. Most of the AEM-DEBFCs show an OCV close to 1.0 V while the DBFC using the Co-impregnated PVA-AER membrane shows an OCV as high as 1.11 V. The addition of a small amount of catalyst in the membrane can reduce the electrode polarization thus increase the OCV. It should be noted that OCV is related to the operating temperature, the concentration of the fuel, gas pressure at the cathode and the fuel cross-over. The higher OCV observed is likely related to the decreased fuel cross-over although the influence of other parameters cannot be completely ruled out. Therefore, the multi-functionalization of the membrane provides a new strategy for the design of high-performance DBFC. Potentially this approach can be applied to other types of fuel cells too. For a fuel cell using gaseous fuels such as hydrogen, cross-over is not a major concern then the benefits of high ionic conductivity and reduced polarization resistance at the electrodes of this new type of membrane electrolyte will be more significant.

5. Conclusions

In summary, it was found that addition of a Co-based catalyst in the PVA-AER composite membrane can significantly increase the ionic conductivity, decrease the electrode polarization and reduce the fuel cross-over. The DBFCs using the Co-impregnated PVA-AER membrane show a high OCV of 1.11 V and a power density of 283 mW cm^{-2} at 60 °C which is much higher than those for DBFCs using pure PVA-AER membrane as the electrolytes. The idea of adding catalyst in the electrolyte membrane has been demonstrated in this work, and this will

provide a new strategy in developing high-performance fuel cells. It may find a wide range of potential applications in fuel cells and other electrochemical devices.

Acknowledgment

The authors wish to thank Dr. Aiguo Li and Juan Wang in BL15U1 of Shanghai Synchrotron Radiation Facilities, Dr. Hongzhong Chi and Huangliang Ni in Hangzhou Dianzi University. This work is financially supported by the Zhejiang Provincial Natural Science Foundation of China (No. LR14B060002 and LY18B060005), the National Natural Science Foundation of China (No.11605280) and EPSRC (No. EP/G030995/1), the Natural Science Foundation of Shanghai (17ZR1436800).

Appendix A. Supplementary data

Supplementary data related to this article can be found at http://dx.doi.org/10.1016/j.jpowsour.2017.11.008.

References

[1] S. Moghaddam, E. Pengwang, Y.-B. Jiang, A.R. Garcia, D.J. Burnett, C.J. Brinker, et al., Nat. Nanotechn 5 (2010) 230–236.
[2] R. Borup, J. Meyers, B. Pivovar, Y.S. Kim, R. Mukundan, N. Garland, et al., Chem. Rev. 107 (2007) 3904–3951.
[3] Y.-J. Wang, J. Qiao, R. Baker, J. Zhang, Chem. Soc. Rev. 42 (2013) 5768–5787.
[4] W. Xu, Z.C. Wu, S.W. Tao, J. Mater Chem. A 4 (2016) 16272–16287.
[5] J. Pan, C. Chen, Y. Li, L. Wang, L. Tan, G. Li, et al., Energy Environ. Sci. 7 (2014) 354–360.
[6] J.R. Varcoe, P. Atanassov, D.R. Dekel, A.M. Herring, M.A. Hickner, P.A. Kohl, et al., Energy Environ. Sci. 7 (2014) 3135–3191.
[7] T. Palaniselvam, V. Kashyap, S.N. Bhange, J.-B. Baek, S. Kurungot, Adv. Funct. Mater 26 (2016) 2150–2162.
[8] Z. Yang, R. Guo, R. Malpass-Evans, M. Carta, N.B. McKeown, M.D. Guiver, et al., Angew. Chem. Int. Ed. 55 (2016) 11499–11502.
[9] G. Couture, A. Alaaeddine, F. Boschet, B. Ameduri, Prog. Poly Sci. 36 (2011) 1521–1557.
[10] C.-M. Chang, H.-Y. Li, J.-Y. Lai, Y.-L. Liu, RSC Adv. 3 (2013) 12895–12904.
[11] C.-F. Lo, J.-F. Wu, H.-Y. Li, W.-S. Hung, C.-M. Shih, C.-C. Hu, et al., J. Memb. Sci. 444 (2013) 41–49.
[12] R. Lan, S.W. Tao, J.T.S. Irvine, Energy Environ. Sci. 3 (2010) 438–441.
[13] R. Lan, S.W. Tao, J Power Sources 196 (2011) 5021–5026.
[14] D.A. Werner, C.C. Huang, D. Aminoff, Anal. Biochem. 54 (1973) 554–560.
[15] C.-C. Huang, Y.-L. Liu, W.-H. Pan, C.-M. Chang, C.-M. Shih, H.-Y. Chu, et al., J. Poly Sci. B 51 (2013) 1779–1789.
[16] H.Y. Qin, Z.X. Liu, L.Q. Ye, J.K. Zhu, Z.P. Li, J. Power Sources 192 (2009) 385–390.
[17] J. Yang, H. Hyodo, K. Kimura, T. Sasaki, Nanotechnology 21 (2009) 045605.
[18] C.-C. Yang, J. Memb. Sci. 288 (2007) 51–60.
[19] C.C. Yang, Y.J. Li, S.J. Chiu, K.T. Lee, W.C. Chien, C.A. Huang, J. Power Sources 184 (2008) 95–98.
[20] T.J. Peckham, S. Holdcroft, Adv. Mater 22 (2010) 4667–4690.
[21] P.-Y. Olu, N. Job, M. Chatenet, J. Power Sources 327 (2016) 235–257.
[22] J. Ma, N.A. Choudhury, Y. Sahai, Renew. Sustain. Energy Rev. 14 (2010) 183–199.
[23] X. Yuan, H. Wang, J. Colin Sun, J. Zhang, Int. J. Hydrogen Energy 32 (2007) 4365–4380.
[24] S.-W.C. Ryan O'Hayre, Whitney Colella, Fritz B. Prinz, 3 rd, Hoboken (Ed.), Fuel Cell Fundamentals, third ed., Wiley, 2016.
[25] X. Yuan, J.C. Sun, H. Wang, J. Zhang, J. Power Sources 161 (2006) 929–937.
[26] X. Yang, Y. Liu, S. Li, X. Wei, L. Wang, Y. Chen, Sci. Rep. 2 (2012) 567.
[27] J.H. Wee, J. Power Sources 155 (2006) 329–339.
[28] R. Jamard, J. Salomon, A. Martinent-Beaumont, C. Coutanceau, J. Power Sources 193 (2009) 779–787.
[29] R. Jamard, A. Latour, J. Salomon, P. Capron, A. Martinent-Beaumont, J. Power Sources 176 (2008) 287–292.
[30] C. Qu, H. Zhang, F. Zhang, B. Liu, J. Mater Chem. 22 (2012) 8203–8207.
[31] Z. Mai, H. Zhang, X. Li, X. Geng, H. Zhang, Electrochem Comm. 13 (2011) 1009–1012.
[32] D. Chen, S. Yu, X. Liu, X. Li, J. Power Sources 282 (2015) 323–327.
[33] J. Ma, N.A. Choudhury, Y. Sahai, R.G. Buchheit, Fuel Cells 11 (2011) 603–610.
[34] M. Figlarz, J. Guenot, Tournemo.Jn. J Mater Sci. 1974;9:772–776.
[35] V. Pralong, A. Delahaye-Vidal, B. Beaudoin, B. Gerand, J.M. Tarascon, J. Mater Chem. 9 (1999) 955–960.
[36] R.S. Malik, U. Soni, S. Singh Chauhan, P. Verma, V. Choudhary, RSC Adv. 6 (2016) 47536–47544.